UNIVERSITY OF BARCELONA

MASTER THESIS

Adiabatic quantum algorithm for the Bose-Hubbard model

Author:
María Cea Fernández

Supervisor:
Axel Pérez-Obiol

Quantic
Barcelona Supercomputing Centre

July 11, 2022

Adiabatic quantum algorithm for the Bose-Hubbard model

María Cea Fernández

Supervised by: Axel Pérez-Obiol

Barcelona Supercomputing Centre, 08034 Barcelona

11 July 2022

In recent years research has been carried out on algorithms to simulate quantum many body systems in current NISQ devices. In particular, for the ground state finding problem, known to be QMA-complete, a quantum adiabatic algorithm can be used. On the other hand, the Bose-Hubbard model has gained impact lately because of the prediction of exotic phases of matter and because its experimental realisation in a set up with cold atoms in optical lattices. In this work, an adiabatic quantum algorithm is designed to obtain the ground state of a one-dimensional Bose-Hubbard model. The three parts of the algorithm are presented: initial state preparation, adiabatic evolution and measurement. The results presented correspond to a system of 2 sites and N_P particles, although the algorithm has been tested for systems with more sites. The algorithm has been tested by performing simulations.

Keywords: TFM, Quantum, Barcelona, Adiabatic, Bose-Hubbard, STA

Acknowledgements

I am grateful to my supervisor Axel Pérez-Obiol for useful discussions as well as all the members of my research group. I also acknowledge support from Barcelona Supercomputing Centre.

María Cea Fernández: mceafern@bsc.es

Contents

1 Introduction

Quantum simulation of physical systems with a quantum computer has gained importance during the last few years. Simulating a quantum many-body system on a classical computer requires a number of operations that grows exponentially with the number of degrees of freedom of the system but it is believed that quantum computers can solve them more efficiently [SOKG03]. Scientific progress has led to the first noisy intermediate-scale quantum NISQ devices [BCLK+21]. Although they have limitations (number of qubits available, gate fidelity, circuit depth) and are still a long way from being efficient problem solvers, algorithms are being developed to see if they would provide a quantum advantage [STC22].

The ground state finding problem belongs to the QMA-complete class, which is the analogue of NP-complete for a quantum computer. However, there are some promising heuristics. First, there is the quantum approximate optimization algorithm (QAOA). This method is within the variational algorithms (VQA), which are based on one of the most used principles in physics: the variational principle. Another is the quantum adiabatic algorithm (QAA). This consists of starting from the ground state of a known Hamiltonian and slowly varying its parameters to obtain the desired Hamiltonian. If this evolution is done in a sufficiently long time T, the ground desired is reached. Recently a new method has been proposed that combines the two previous ones, the variational quantum quantum adiabatic algorithm (VQAA) [STC22]. However, in this work we will focus on the quantum adiabatic algorithm.

Most algorithms for solving the many-body problem have focused on spin 1/2 or fermionic systems, to simulate chemical electronic structure, nuclear structure and condensed matter physics. Qubit-based quantum computation is the most widespread and that is why these are the systems that have been studied the most. However, there are many physical problems of interest with d-level particles (qudits): bosonic fundamental particles, vibrational modes, spin-s particles, or electronic energy levels in molecules and quantum dots. In order to map a system of d levels to a set of qubits, an integer is assigned to each of the d levels so that one has an integer-to-bit mapping. Possible encodings include Standard binary, Gray code and unary encoding [SMK+20].

The Bose-Hubbard model (BH), originally introduced to describe condensed matter problems, has gained high impact with its experimental realization in a set up with cold atoms in optical lattices [RGLJD17]. In addition, recent experiments have shown the creation of a state of matter where ordered material can flow without friction, an exotic phase known as supersolid [SMK+20]. Although different techniques are able to capture ground state properties of the Bose-Hubbard Hamiltonian, with classical techniques it is intractable to solve its full spectrum. This can be done with exact diagonalization (EC) techniques, but restricted to small many-body systems [RGLJD17]. Simulating BH models on a quantum computer can help to study the behavior of these systems near quantum phase transitions, a very complicated regime to study with a classical computer, as well as to predict unknown phases [SMK+20].

In this work, an adiabatic quantum algorithm is proposed to find the ground of a one-dimensional Bose-Hubbard model. The Bose-Hubbard model is described in Section 2 by way of introduction. Section 3 shows a description of the algorithm: first algorithms for the preparation of the initial state are proposed, then the adiabatic evolution using Trotterization is presented and finally a measurement strategy is explained. In all these subsections, the scaling of each of the algorithms is analyzed. In addition, a shortcuts to adiabaticity (STA) method is proposed to accelerate the evolution process and reduce the depth of the circuit. In Section 4 we develop the numerical results obtained and compare

the simulations without STA and with STA for some examples, discussing the possible advantages of this method. We conclude with a summary of the work and the possible future lines of research it leaves open.

2 Bose-Hubbard model

The Hamiltonian of the one dimensional Bose-Hubbard model can be written as:

$$\hat{\mathcal{H}}_{BH} = \underbrace{\frac{U}{2}\sum_{i=1}^{N_S}\hat{n}_i(\hat{n}_i-1)}_{\text{interaction term}} \underbrace{-t\sum_{\langle ij\rangle}\left(\hat{a}_i^\dagger\hat{a}_j+\hat{a}_j^\dagger\hat{a}_i\right)}_{\text{hoppping term}} -\mu\sum_{i=1}^{N_S}\hat{n}_i, \tag{1}$$

where $\hat{a}_i^\dagger$ and $\hat{a}_i$ are creation and annihilation operator respectively, $\hat{n}_i = \hat{a}_i^\dagger\hat{a}_i$ is the particle number operator and N_S is the total number of the sites.

The first part is the *interaction (Coulomb) term*, $\hat{\mathcal{H}}_C$, which describes the on-site interaction of the boson. It has the same form as the electrostatic energy of N_S electric charges. In the second part, $\hat{a}_i^\dagger\hat{a}_j$ means that one boson is annihilated at site j and then created at site i, so the net effect is this boson "moves" from j to i. That's why we call it *hopping (kinetic) term*, $\hat{\mathcal{H}}_K$. Summation indices $\langle ij\rangle$ means that only neighboring lattice sites are considered, since the particles can't move too far. Periodic boundary conditions are assumed. The *chemical* potential μ in the last part essentially sets the total number of particles. If the number is fixed, then it will become a constant and we can simply ignore it. For more details about the ground state of the Coulomb and kinetic terms, see Appendix A.

A convenient finite basis, with a fixed number of particles N_P, is given by the states of the Fock space restricted to N_P particles,

$$|n_1, n_2, \ldots, n_i, \ldots, n_{N_S}\rangle\,, \tag{2}$$

where N_S is the number of sites and $N_P = \sum_{i=1}^{N_S} n_i$. The number of ways of placing N_P particles in N_S sites is (see Table 1) [RGLJD17],

$$\mathcal{N}_{N_P}^{N_S} = \binom{N_P+N_S-1}{N_P} = \frac{(N_P+N_S-1)!}{N_P!(N_S-1)!}. \tag{3}$$

The large growth of the size of the Hilbert space with N_P and N_S is a motivation to search for new methods to study this problem. In this work we present results for two-site systems ($N_S = 2$), for which the Hamiltonian is explicitly written as

$$\hat{\mathcal{H}}_{BH}(N_S=2) = \frac{U}{2}\left[\hat{n}_1(\hat{n}_1-1)+\hat{n}_2(\hat{n}_2-1)\right] - t\left(\hat{a}_1^\dagger\hat{a}_2+\hat{a}_2^\dagger\hat{a}_1\right). \tag{4}$$

Restricting ourselves to two sites influences the preparation of the initial state, but the remaining parts of the algorithm are easily generalizable. We can fix t without losing generalization and leave U as a parameter. Furthermore, we take $U = 1$ arbitrarily. The algorithm does not depend on this choice and simulations would only change at a qualitative level.

	N_S												
N_P	**1**	**2**	**3**	**4**	**5**	**6**	**7**	**8**	**9**	**10**	**11**	**12**	**13**
1	1	2	3	4	5	6	7	8	9	10	11	12	13
2	1	3	6	10	15	21	28	36	45	55	66	78	91
3	1	4	10	20	35	56	84	120	165	220	286	364	445
4	1	5	15	35	70	126	210	330	495	715	1001	1365	1820
5	1	6	21	56	126	252	462	792	1287	2002	3003	4368	6188
6	1	7	28	84	210	462	924	1716	3003	5005	8008	12376	18564
7	1	8	36	120	330	792	1716	3432	6435	11440	19448	31824	50388
8	1	9	45	165	495	1287	3003	6435	12870	24310	43758	75582	125970
9	1	10	55	220	715	2002	5005	11440	24310	48620	92378	167960	293930
10	1	11	66	286	1001	3003	8008	19448	43758	92378	184756	352716	646646
11	1	12	78	364	1365	4368	12376	31824	75582	167960	352716	705432	1352078
12	1	13	91	455	1820	6188	18564	50388	125970	293930	646646	1352078	2704156
13	1	14	105	560	2380	8568	27132	77520	203490	497420	1144066	2496144	5200300

Table 1: Size of the Hilbert space for N_P bosons in N_S sites for $N_P,\ N_S = 1, \cdots, 13$.

3 Description of the algorithm

In this work we study how to implement a Bose-Hubbard model in a quantum computer. The algorithm consists of three parts: first, the problem is mapped to a quantum computer, in this case using the Gray code. Second, a state is generated that will act as the initial state for its subsequent adiabatic evolution ($IGSP$). Then, this initial state undergoes adiabatic evolution (AE) until it approaches the target state with high fidelity. Following this evolution, the necessary basis changes are applied to measure the final energy in the most efficient way possible.

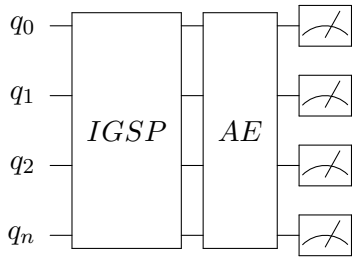

Figure 1: Circuit implementation for the digitized adiabatic evolution. First, the initial state is prepared ($IGSP$). Then it is subjected to adiabatic evolution (AE). Finally, measurements are made to obtain expected values.

3.1 Gray code mapping

The first step of the algorithm is to map the Fock basis states to qubits in a quantum computer. Each state is written in terms of integers defining the number of particles in each site, see Ec(2). There are many ways to map integers with N_q bit strings such as Standard Binary, Gray or Unary. The particularity of the Gray code is that between two consecutive numbers only one bit changes; that is, the Hamming distance d_H (number of mismatched bits between two bit strings) between two consecutive integers is 1. In

other words, moving between adjacent integer requires only one bit flip (see Table 2). This encoding is suitable for tridiagonal operators, since all non-null elements have $d_H = 1$ [SMK+20]. Hopping terms such as $\hat{\mathcal{H}}_K$ are tridiagonal operators (first neighbors approach), i.e, containing terms like $|I\rangle\langle I+1| + |I+1\rangle\langle I|$. Each integer is encoded as

$$|I\rangle \to |x_{n_q-1}\rangle \cdots |x_0\rangle\,, \qquad x_i \in \{0,1\}.$$

One then converts each qubit-local term $|x_i\rangle\langle x_i'|$ to qubit operators using the following four expressions:

$$\begin{aligned} |0\rangle\langle 0| &= \frac{1}{2}(\mathbb{I}+Z) \equiv \hat{\sigma}^0, & |1\rangle\langle 1| &= \frac{1}{2}(\mathbb{I}-Z) \equiv \hat{\sigma}^1 \\ |0\rangle\langle 1| &= \frac{1}{2}(X+iY) \equiv \hat{\sigma}^+, & |1\rangle\langle 0| &= \frac{1}{2}(X-iY) \equiv \hat{\sigma}^-. \end{aligned} \tag{5}$$

Operators $\hat{a}_i^\dagger$ and $\hat{a}_i$ appearing in Ec.(1) can be written in terms of $\hat{\sigma}^j$, see Ec.(5) and, therefore, in terms of Pauli strings: $\hat{a}_i^\dagger \hat{a}_j = \sum_k c_k A_0 \otimes A_1 \otimes \cdots \otimes A_{N_q}$, where $A_l = \{X_l, Y_l, Z_l\} \cup \{\mathbb{I}\}$. The number of qubits N_q needed to represent a system of N_S sites and N_P particles in Gray is given by $N_q = N_S n_q$, where $n_q = \lfloor 1 + \log_2 N_P \rfloor$ is the number of qubits representing one site.

For any mismatched qubit i, i.e, any qubit for which $x_i \neq x_i'$ the qubit-local term contains two Pauli operators. For matched qubits ($x_i = x_i'$), instead has one identity and one Pauli operator (in this work the set of Pauli matrices is defined to exclude the identity). The more Pauli operators there are, the more operations to implement. That is what motivates us to use this encoding [SMK+20].

3.2 Initial state preparation

The initial state preparation consists of constructing a circuit by applying unitary gates in such a way that the ground state of the initial Hamiltonian $\hat{\mathcal{H}}_i$ is obtained. The Hamiltonian has two terms of which we know how to compute the ground state theoretically, see Appendix A. The Coulomb term $\hat{\mathcal{H}}_C$ is diagonal when expressed in Fock basis and $\hat{\mathcal{H}}_K$ is diagonal when expressed in momentum basis, see Ec.(A.12). Each term of the Hamiltonian commutes with particle number operator, i.e $\left[\hat{\mathcal{H}}_C, \hat{N}\right] = \left[\hat{\mathcal{H}}_K, \hat{N}\right] = 0$, which means that the number of particles is conserved [1]. As a result the whole evolution will happen within a subspace within the full Hilbert space.

[1] Particle number operator $\hat{N}$ is defined as $\hat{N} = \sum_{i=1}^{N_S} \hat{n}_i$.

Decimal	SB	Gray	Unary
0	0000	0000	000000000001
1	0001	0001	000000000010
2	0010	0011	000000000100
3	0011	0010	000000001000
4	0100	0110	000000010000
5	0101	0111	000000100000
6	0110	0101	000001000000
7	0111	0100	000010000000
8	1000	1100	000100000000
9	1001	1101	001000000000
10	1010	1111	010000000000
11	1011	1110	100000000000

Table 2: The standard binary (SB), Gray code, and unary encodings.

In this section we will present an algorithm for the preparation of the initial state in Gray if we take $\hat{\mathcal{H}}_C$ as the initial Hamiltonian, as well as another to prepare the ground state of $\hat{\mathcal{H}}_K$. We will see that if we choose the former the state is easy to prepare, especially for an even number of particles. However, if we choose the latter instead, the preparation becomes a complicated task.

Ground state of $\hat{\mathcal{H}}_C$

The ground state of $\hat{\mathcal{H}}_C$ in the Fock basis is

$$|\Psi_C(N_P)\rangle = \begin{cases} \left|\frac{N_P}{2}\,\frac{N_P}{2}\right\rangle, & if \quad N_P \text{ is even} \\ \frac{1}{\sqrt{2}}\left(\left|\frac{N_P}{2}-\frac{1}{2}\,\frac{N_P}{2}+\frac{1}{2}\right\rangle + \left|\frac{N_P}{2}+\frac{1}{2}\,\frac{N_P}{2}-\frac{1}{2}\right\rangle\right), & if \quad N_P \text{ is odd.} \end{cases} \tag{6}$$

Although the ground state for an odd number of particles is degenerate, by doing first-order perturbation theory it can be seen that this superposition state of Eq.6 is the one that allows to obtain the target state after adiabatic evolution, see Appendix A.

For the case of an even number of particles it is only necessary to apply an X gate on qubits that have to be in $|1\rangle$ and the depth of the circuit is always constant and equal to 1. For instance,

$$|\Psi_C(N_P=12)\rangle = |6\,6\rangle\,, \qquad\qquad |\Psi_C^{(G)}(N_P=12)\rangle = |101\,101\rangle\,,$$

and only one X gate has to be applied on qubits q_0, q_2, q_3 and q_5.

For the case of and odd number of particles the circuit construction is slightly different as a superposition state has to be prepared. The algorithm to be applied is as follows:

- (Step 1): Qubits that are in the same state (q_{C_i}) are identified for the two product states. Note that the Gray code makes all but one state common, i.e. the number of uncommon states (q_{U_j}) will be equal to 2 (for $N_S = 2$).

$$|q_{C_1} q_{C_2} \cdots q_{C_{n-2}}\rangle \otimes \frac{1}{\sqrt{2}}\left(|q_{U_1} q_{U_2}\rangle + |q_{U_2} q_{U_1}\rangle\right).$$

- (Step 2): X gates are applied to common qubits in state $|1\rangle$.
- (Step 3): A Hadamard gate is applied on the first non-common qubit, q_{U_1}.
- (Step 4): A $CNOT$ gate is applied, with q_{U_1} being the control qubit and q_{U_2} the target qubit.
- (Step 5) An X gate is applied on the non-common qubit not in the desired state.

For instance,

$$|\Psi_C(N_P=5)\rangle = \frac{1}{\sqrt{2}}\left(|2\,3\rangle + |3\,2\rangle\right), \qquad |\Psi_C^{(G)}(N_P=5)\rangle = \frac{1}{\sqrt{2}}\left(|11\,10\rangle + |10\,11\rangle\right).$$

The state is separated as follows

$$|q_0:1\,q_2:1\rangle \otimes \frac{1}{\sqrt{2}}\left(|q_1:1\,q_3:0\rangle + |q_1:0\,q_3:1\rangle\right).$$

In step 2 we have (following the order of qubits just left in the previous equation)

$$|11\rangle \otimes |00\rangle.$$

When applying the Hadamard gate on q_2,

$$|11\rangle \otimes \frac{1}{\sqrt{2}}\left(|00\rangle + |10\rangle\right).$$

After step 4 we have,

$$|11\rangle \otimes \frac{1}{\sqrt{2}}\left(|00\rangle + |11\rangle\right).$$

Finally, with step 5 we get

$$|11\rangle \otimes \frac{1}{\sqrt{2}}\left(|10\rangle + |01\rangle\right).$$

After rearranging the qubits, we have the desired state.
With this algorithm the depth of the circuit is always constant and equal to 3 (for $N_S = 2$).

Ground state of $\hat{\mathcal{H}}_\mathbf{K}$

The (unnormalized) ground state of $\hat{\mathcal{H}}_K$ for $N_S = 2$ in the Fock basis is, see Ec.(A.16)

$$|\Psi_K\rangle = \sum_{i=0}^{N_P} \binom{N_P}{i} \sqrt{i!}\sqrt{(N_P-i)!}\,|i\;N_P-i\rangle. \tag{7}$$

An algorithm has been designed to prepare such states in Gray.
Ultimately, we have to prepare a state of the form

$$|\Psi_K(N_P)\rangle = \sum_{i=0}^{N_P} c_i\,|i, N_P-i\rangle. \tag{8}$$

The idea is to prepare the first part of the state (to prepare the state by ignoring the qubits corresponding to the second site), i.e

$$|\Phi\rangle = \left(\sum_{i=0}^{N_P} c_i \, |i^{(G)}\rangle\right) \underbrace{|00\cdots0\rangle}_{n_q}, \tag{9}$$

working with n_q qubits and to have n_q additional qubits to complete the second part. For this task, we add several n-qubit Toffoli gates. Control qubits are those describing the state of the first site and target qubits those corresponding to the second site. It is then a task of adding as many n-qubit Toffoli gates as necessary to obtain the desired superposition state.

The algorithm is as follows. First $n_q - 2$ controlled-R_y gates are applied on the first $n_q - 2$ qubits: one rotation in q_0, two rotations on q_1 controlled by q_0, four rotations on q_2 controlled by q_0 and q_1 and so on. Then 2^{n_q-1} circuits like the one in Fig.13 controlled by the $n_q - 2$ qubits are concatenated. Finally, as many $(n_q + 1)$-qubit Toffoli gates are added as many qubits of the second site have to modify their state from $|0\rangle$ to $|1\rangle$ (for all the states that make up the initial state).

For the reader's clarity, a specific example has been explained in detail in appendix C. An explanation of the scaling of this algorithm with the number of particles is also given in the appendix.

The depth of this circuit as a function of the number of particles N_P is given by (see Appendix C),

$$\mathcal{D}_K^{(\mathrm{IGS})} \leq 227 - 239N_P + 4\log_2 N_P \left[(-16 + 27N_P) + 2N_P \log_2 N_P\right], \tag{10}$$

i.e, it scales polinomially with the number of particles N_P.

The reason for the faster depth growth for this algorithm is because n-qubit Toffoli gates can be decomposed into two-qubit controlled-rotation gates, having a depth of $8n-20$ [SP13].

It is evident then that it is more convenient to choose $\hat{\mathcal{H}}_C$ as the initial Hamiltonian since it involves a significantly simpler initial state preparation with constant depth with N_P.

Starting from $\hat{\mathcal{H}}_C$ or $\hat{\mathcal{H}}_K$ implies, in addition to a different initial state preparation, a more or less efficient adiabatic evolution. This depends strongly on the overlap of the initial state with the target state. Starting from $\hat{\mathcal{H}}_K$ the initial overlap is quite high, which will be advantageous for adiabatic evolution. Starting from $\hat{\mathcal{H}}_C$ there is a difference between the case of even and odd particles. In the former the state is quite far from the final one, which will slow down the subsequent evolution. In the latter it gets better.

In the following section it will be the choice of $\hat{\mathcal{H}}_K$ as the initial Hamiltonian that will be the most advantageous option, thus showing the pros and cons of considering both choices. At the end of this section a new way of dealing with adiabatic evolution will be proposed by introducing shortcuts to adiabaticity (STA) in such a way that it will be easier to choose one of them.

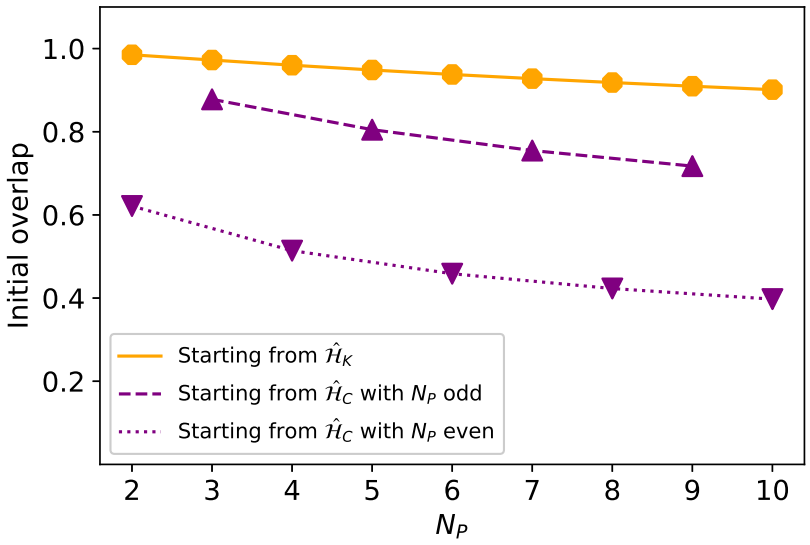

Figure 2: Overlap between the initial state and the target state starting from the $\hat{\mathcal{H}}_C$ ground state in purple with an odd number of particles (dashed line) and with an even number of particles (dotted line), and starting from the $\hat{\mathcal{H}}_K$ ground state in orange (solid line). The initial fidelity is computed as $\mathcal{F}_i = |\langle\psi_i|\psi_f\rangle|^2$.

3.3 Adiabatic evolution

The way we want to obtain the ground state energy of the one-dimensional Bose-Hubbard Hamiltonian is by adiabatic evolution. As stated by Born and Fock (1928) in the adiabatic theorem: "a physical system remains in its instantaneous eigenstate when a given perturbation is acting on it slowly enough and if there is a gap between the eigenvalue and the rest of the Hamiltonian's spectrum" [TIMG+13]. Therefore, if we know the ground state of a given Hamiltonian, we can slowly modify the latter until we finally obtain the Hamiltonian we want to study. If the evolution is slow enough, at the end of the process we will have reached the ground state of the target Hamiltonian with high fidelity. The evolution time must be at least $\mathcal{O}(g^2)$ where g is the gap between the ground and first-excited states [POPSSR+22]. For a truly adiabatic process we require the evolution time T satisfies $T \to \infty$.

It is important to choose the initial Hamiltonian well: we must try to prevent its ground state from being degenerate. The ground state of the kinetic term, $\hat{\mathcal{H}}_K$ is non-degenerate for any number of sites and particles, see Appendix A. However, the ground state of the Coulomb term, $\hat{\mathcal{H}}_C$ is degenerate for an odd number of particles, see Appendix A.
Following the general method for Adiabatic Quantum Computing (AQC), we express the Hamiltonian at time t as a combination of two time-independent parts:

$$\hat{\mathcal{H}}(t) = (1 - \lambda(t))\hat{\mathcal{H}}_i + \lambda(t)\hat{\mathcal{H}}_f, \tag{11}$$

where $\hat{\mathcal{H}}_i$ and $\hat{\mathcal{H}}_f$ are time-independent with ground states $|\psi_i\rangle$ and $|\psi_f\rangle$, respectively. The time dependence of the system is introduced through the parameter $\lambda(t)$. AQC allows $\lambda(t)$ to be a function that varies from 0 to 1 and drives the system from $|\psi_i\rangle$ to $|\psi_f\rangle$. Let's choose it as a linear function, $\lambda(t) = t/T$, with T being the total evolution time.
To perform the state evolution, the Schrödinger equation with the above time-dependent

Hamiltonian is applied[2]

$$|\psi(T)\rangle = \hat{\mathcal{T}} e^{-i\int_0^T \mathcal{H}(t)dt} |\psi(0)\rangle \,. \tag{12}$$

We can approximate this solution if we discretize the evolution,

$$|\psi(T)\rangle \approx \prod_{j=0}^{N} e^{-i\mathcal{H}(j\delta t)\delta t} |\psi(0)\rangle \,, \tag{13}$$

where $\delta t = T/N$ is the time taken in each step.

So that adiabatic evolution does not involve very long times, it is interesting to start from an initial state that is not too far from the target state. As mentioned at the end of the previous section, it will be $\hat{\mathcal{H}}_K$ that will be suitable for reducing the number of trotter steps. It is also important to know how to set the parameters T, N and δt (one depends on the other two) to obtain the highest possible fidelity in the smallest number of N steps.

For the algorithm to work on a quantum computer, operators of the form $e^{-i\mathcal{H}(j\delta t)\delta t}$ have to be decomposed into available operations. In order to apply each adiabatic step in the quantum circuit we use Trotterization, which consists of applying each term of the Hamiltonian separately [POPSSR+22]

$$e^{-i\hat{\mathcal{H}}t} = e^{-i\hat{\mathcal{H}}_C t} e^{-i\hat{\mathcal{H}}_K t} + \mathcal{O}(\left[\hat{\mathcal{H}}_C, \hat{\mathcal{H}}_K\right], \delta t^2). \tag{14}$$

If $\hat{\mathcal{H}}_i = \hat{\mathcal{H}}_C$

$$e^{-i\hat{\mathcal{H}}(j\delta t)\delta t} \approx e^{-i\hat{\mathcal{H}}_C \delta t} e^{-i\hat{\mathcal{H}}_K \frac{j}{N}\delta t}, \tag{15}$$

and if $\hat{\mathcal{H}}_i = \hat{\mathcal{H}}_K$ then:

$$e^{-i\hat{\mathcal{H}}(j\delta t)\delta t} \approx e^{-i\hat{\mathcal{H}}_K \delta t} e^{-i\hat{\mathcal{H}}_C \frac{j}{N}\delta t}. \tag{16}$$

Since $\hat{\mathcal{H}}_C$ and $\hat{\mathcal{H}}_K$ can be written in terms of Pauli matrices, in the end we are left with a product of exponentials of Pauli strings for each Trotter step. In each of these the coefficients accompanying each Pauli string varies.

According to [SMK+20], although there are several methods to approximate Ec.(13) including Suzuki-Trotter methods, recent results suggest that simple first-order Trotterization will have lower error for near- and medium-term hardware, even if the other methods are asymptotically more efficient.

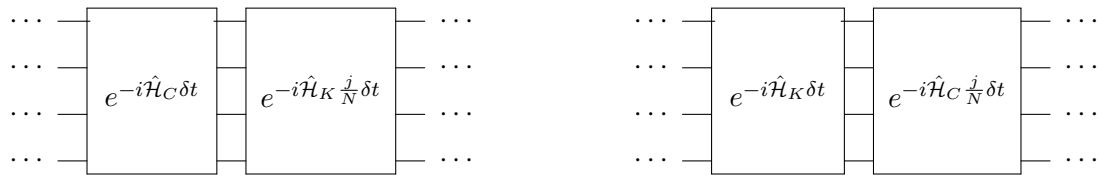

(a) (b)

Figure 3: Implementation of the j^{th} trotter step in a quantum circuit with (a) $\hat{\mathcal{H}}_i = \hat{\mathcal{H}}_C$ and (b) $\hat{\mathcal{H}}_i = \hat{\mathcal{H}}_K$. Note that each of these N_q-qubit gates is the concatenation of circuits as shown in Fig.4.

[2]We define $|\psi(T)\rangle \equiv |\psi_f\rangle$ and $|\psi(0)\rangle \equiv |\psi_i\rangle$.

The next step consists of translating each Pauli strings exponential into small quantum circuits that we will later concatenate. These unitary operators are implemented in the circuit model.

One needs $2(p-1)$ two-qubit gates for such an operation, where p is the number of Pauli operators in the term [SMK+20] and $p \leq N_q$. Therefore $n(CNOT) \leq 2(N_q - 1)$. There is also a rotation gate $R_z(\theta)$. Depending on whether there are X or Y Pauli matrices, Hadamard and phase gates must be added at the beginning and end of the circuit (a Hadamard gate is added in both cases while a phase gate is only added if there is an Y Pauli matrix). Assuming there is at least one X or Y Pauli matrix, we have an additional depth of 2 (the Hadamard gate can be combined with the phase gate in a single one-qubit gate). Taking into account that for $N_S = 2$ we have $N_q = 2\lfloor(1 + \log_2 N_P\rfloor)$, we have an upper limit for the depth of any such circuit,

$$\mathcal{D}^{(PS)} \leq 5 + 4\log_2 N_P. \tag{17}$$

We now estimate an upper bound for the number of Pauli strings that make up the Hamiltonian. In the BH model for two sites, we have four terms that can be expressed in terms of kronecker products of $\hat{\sigma}^k$ matrices, i.e, $\hat{a}_1^\dagger \hat{a}_1$, $\hat{a}_2^\dagger \hat{a}_2$, $\hat{a}_1^\dagger \hat{a}_2$, $\hat{a}_2^\dagger a_1$. Each of these terms contain N_P number of kronecker products. The kronecker products are given between N_q number of matrices. Each of the matrices is decomposed into a sum of two Pauli matrices, see Eq.(5). Therefore, the number of Pauli strings will be given by $4N_P 2^{N_q}$. But $2^{N_q} \leq 4N_P^2$. Hence,

$$n(PS) \leq 16N_P^3. \tag{18}$$

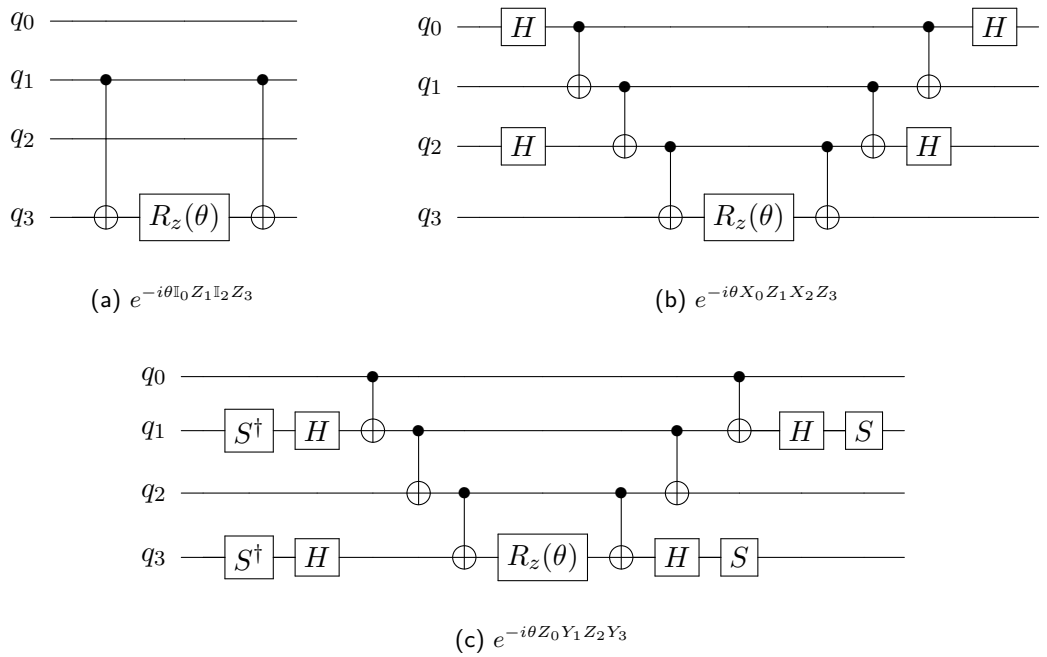

(a) $e^{-i\theta \mathbb{I}_0 Z_1 \mathbb{I}_2 Z_3}$

(b) $e^{-i\theta X_0 Z_1 X_2 Z_3}$

(c) $e^{-i\theta Z_0 Y_1 Z_2 Y_3}$

Figure 4: Some examples of the implementations of unitary operators with the form $e^{-i\theta A_0 A_1 A_2 A_3}$, where $A_j = \{X_j, Y_j, Z_j\} \cup \{\mathbb{I}\}$. One needs $2(p-1)$ two qubit-gates for such an operation [SMK+20], where p is the number of Paui operators in the term.

With this we can also know an upper dimension for the depth of a trotter step

$$\mathcal{D}^{(TS)} \leq 16N_P^3(5 + 4\log_2 N_P). \tag{19}$$

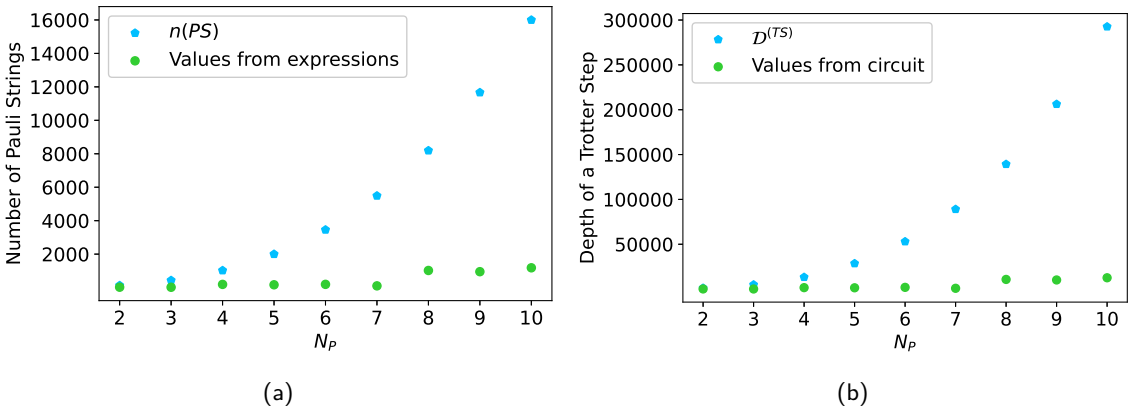

Figure 5: (a) Number of Pauli strings that make up the Hamiltonian and (b) their associated depth of a trotter step for different number of particles. In blue are the points corresponding to the theoretically calculated upper limit and in green are the values extracted directly from (a)the explicit expressions and (b) the constructed circuits.

The discrepancy for the number of Pauli strings is actually due to term cancellations when developing the kronecker products of the form $\hat{\sigma}_0^k \otimes \cdots \otimes \hat{\sigma}_{N_q}^l$ into products of Pauli matrices. In addition, concatenating circuits like the one in Fig.4 results in gate cancellation, which leads to a decrease in the depth of a trotter step.

STA with approximate counter-diabatic driving

The idea of this subsection is to implement an STA to make the adiabatic evolution faster and thus achieve a lower number of trotter steps. Moreover, if it is fast enough we could use $\hat{\mathcal{H}}_C$ as the initial Hamiltonian and thus avoid the complicated initial state preparation if we take $\hat{\mathcal{H}}_K$.

Counterdiabatic (CD) driving is a way to generate adiabatic dynamics without the need for long times: excitations due to non-adiabaticity are accurately compensated by adding an extra term to the Hamiltonian. However, although this term is known and is given by the adiabatic gauge potential[3], obtaining it for many-body systems is complicated since it requires knowing the spectrum of the instantaneous Hamiltonians [CPSP19]. Recently, a new way to obtain this gauge potential has been proposed by using the nested commutator (NC) [HPD+21],

$$\hat{\mathcal{A}}_\lambda^{(l)} = i \sum_{k=1}^{l} \alpha_k(t) \left[\hat{H}, \left[\hat{H}, \cdots \left[\hat{H}, \partial_\lambda \hat{H}\right]\right]\right], \tag{20}$$

where l determines the order of the expansion and there are $2k-1$ nested commutators in each term. The exact gauge potential is obtained in the limit $l \to \infty$. Instead, we consider a finite value of l and treat the expansion coefficients as variational parameters, which can be obtained by minimizing the action S_l:

[3] *Adiabatic gauge potentials* are generators of the unitary transformations relating the eigenstates $|m(\lambda)\rangle$ of $\hat{\mathcal{H}}(\lambda)$ for different values of λ [KSMP17].

$$\mathcal{S}_l = Tr\left[\hat{\mathcal{G}}_l^2\right], \qquad \hat{\mathcal{G}}_l = \partial_\lambda \hat{\mathcal{H}} - i\left[\hat{\mathcal{H}}, \hat{\mathcal{A}}_\lambda^{(l)}\right].$$

If we consider ony the first-order term, our ansatz will be $\hat{\mathcal{A}}_\lambda^{(l)} = i\alpha_1(t)\left[\hat{H}, \partial_\lambda \hat{H}\right]$, and the effective Hamiltonian can be written as

$$\hat{\mathcal{H}}_{eff} = \hat{\mathcal{H}}(\lambda) + \hat{\mathcal{H}}_{CD}, \tag{21}$$

where $\hat{\mathcal{H}}_{CD} = \dot{\lambda}\hat{\mathcal{A}}_\lambda^{(1)}$ is the relevant CD term.

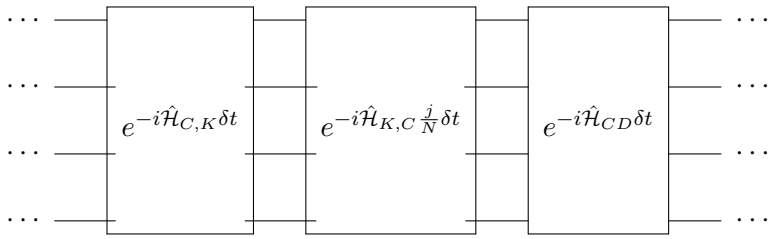

Figure 6: Implementation of the j^{th} trotter step in a quantum circuit using CD driving with. Note that each of these N_q-qubit gates is the concatenation of the circuits in Fig.4.

Using this method, the final ground state is achieved with very few trotter steps compared to digitized adiabatic evolution, which drastically reduces the number of gates required as well as the total simulation time. The price to pay is the increased depth of each trotter step, see Fig.6, as we are adding a new term to the Hamiltonian.

3.4 Measurement

The main objective of the simulation of this system is to calculate the energy of its ground state. To do this, once the adiabatic evolution is performed, we need a measurement procedure to obtain the expected value of the energy ($\langle\hat{\mathcal{H}}_C\rangle_f + \langle\hat{\mathcal{H}}_K\rangle_f$). A minimal set of measurements is obtained by grouping the different parts of the Hamiltonian into terms that commute with each other, so that they can be measured simultaneously.

All Coulomb terms commute with each other and are diagonal. Therefore, obtaining $\langle\hat{\mathcal{H}}_C\rangle$ is straightforward: just measure all the qubits in the z-basis.

$$\begin{aligned}\langle\hat{\mathcal{H}}_C\rangle_f &= \frac{U}{2}\sum_{j=0}^{N_P} jP(j, N_P - j)\left[jP(j, N_P - j) - 1\right] \\ &+ (N_P - j)P(j, N_P - j)\left[(N_P - j)P(j, N_P - j) - 1\right],\end{aligned} \tag{22}$$

where $P(j, N_P - j)$ denotes the probability of obtaining the Fock state $|jN_P - j\rangle$, i.e, $P(j, N_P - j) = \langle jN_P - j|\Psi_f\rangle^2$.

Hopping terms are not diagonal in the computational basis, so a change of basis is necessary to obtain their mean values. In order to reduce the number of measurements to be performed, as well as the depth of the circuits to be introduced for this purpose, we take advantage of the fact that $[X \otimes X, Y \otimes Y] = [X \otimes Y, Y \otimes X] = 0$. Note that if we use Gray encoding, the Pauli strings defining $\hat{\mathcal{H}}_K$ can only have two X or Y matrices. Strings that have

both matrices in the same positions commute. In this way it is possible to simultaneously measure $\{\langle \cdots X_i \cdots X_j \cdots \rangle,\ \langle \cdots Y_i \cdots Y_j \cdots \rangle\}$ and $\{\langle \cdots X_i \cdots Y_j \cdots \rangle,\ \langle \cdots Y_i \cdots X_j \cdots \rangle\}$.

The basis in which $X \otimes X$, $Y \otimes Y$ and $X \otimes Y$, $Y \otimes X$ are simultaneously diagonal are

$$|\Psi^{\pm}\rangle = \frac{1}{2}\left(|00\rangle \pm |11\rangle\right), \qquad |\phi^{\pm}\rangle = \frac{1}{2}\left(|01\rangle \pm |10\rangle\right),$$

and

$$|\Psi'^{\pm}\rangle = \frac{1}{2}\left(|00\rangle \pm i\,|11\rangle\right), \qquad |\phi'^{\pm}\rangle = \frac{1}{2}\left(|01\rangle \pm i\,|10\rangle\right),$$

respectively.

(a) (b)

Figure 7: Circuit introduced to make measurements of (a) $\{\langle \cdots X_i \cdots X_j \cdots \rangle,\ \langle \cdots Y_i \cdots Y_j \cdots \rangle\}$ and (b) $\{\langle \cdots X_i \cdots Y_j \cdots \rangle,\ \langle \cdots Y_i \cdots X_j \cdots \rangle\}$.

For each term in $\hat{\mathcal{H}}_K$, the following probabilities will be obtained P_{00}, P_{01}, P_{10}, P_{11}, where the subscripts refer to the bits of the positions where there are X and/or Y Pauli matrices (i.e. positions i, j). The average value of the terms that make up $\hat{\mathcal{H}}_K$, will be calculated as $c_{00}P_{00} + c_{01}P_{01} + c_{10}P_{10} + c_{11}P_{11}$, where coefficients c_{ij} depend on the change of basis. For the one corresponding to Fig.7a, $c_{00} = c_{01} = +1$ and $c_{10} = c_{11} = -1$ and for the one corresponding to Fig.7b, $c_{00} = c_{11} = -1$ and $c_{01} = c_{10} = +1$.

The number of measurements required is bounded at the top by the number of qubits $1 + N_q$, see Appendix B, and for each of these measurements the maximum depth of the measurement circuit to be implemented is 2 (again we can combine the Hadamard gate with the phase gate of Fig.7b).

4 Simulation and Results

The statevector simulation with *Cirq* is used in this work to perform the circuit evolution of the desired systems.

A code has been built to prepare the initial state according to the algorithms presented in the previous section. Then a circuit corresponding to a Trotter step has been defined, which we concatenate N times depending on the parameters T and δt chosen. Finally, the measurement procedure has been automated by identifying the mean values that can be measured simultaneously and creating accordingly the circuits to be implemented for each measurement. The proposed basis changes for this part have been tested.

To obtain the results presented below, we proceeded as follows. T and δt values have been fixed. For that pair of values we have a number of Trotter steps N to be performed. We start with the state $|0\cdots0\rangle$ and with the function $cirq.final\_state\_vector()$ of *Cirq* we obtain the state after the evolution: first the state $|0\cdots0\rangle$ goes through the preparation circuit of the initial state and then through the N Trotter steps. Once this state is obtained,

the BH Hamiltonian is diagonalized and the overlap between the state obtained through the circuit and the state obtained after diagonalization is calculated. With this we obtain the fidelity. With a quantum computer we do not have access to fidelities, only to energies. To simulate these results we have chosen to represent the fidelities for illustrative purposes, although the behavior of the energies is similar.

The first results here presented comprise the adiabatic evolution from the ground state of $\hat{\mathcal{H}}_C$ and $\hat{\mathcal{H}}_K$ to the full BH model. This evolution can be simulated by applying evolution steps with the full Hamiltonian matrix (adiabatic) for each time step or by decomposing the matrix in simple terms corresponding to one- and two-qubit quantum gates (circuit). The comparison between both methods for several examples is shown in Fig.8. In each case, two periods and two number of steps N are considered.

Figs. 8a, 8b, 8c show the evolution $t = 0 \to 1$, $U = 1$ of $N_P = 2$, $N_P = 3$ and $N_P = 7$ respectively for periods $T = \{1, 3\}$ for $N = \{40, 100\}$. By inspecting the adiabatic evolutions with different periods it is clear that this parameter plays an important role in the evolution. On the other hand, the Trotterization is affected by the number of steps: as N increases, the Trotterized evolution is more similar to the adiabatic one.

The same behaviour is observed in Figs. 8d, 8e and 8f showing the evolution $U = 0 \to 1$, $t = 1$ of $N_P = 2$, $N_P = 3$ and $N_P = 7$ respectively. The only difference is that in this case, the fidelities throughout the evolution are much higher because it starts from an initial state very close to the target one.

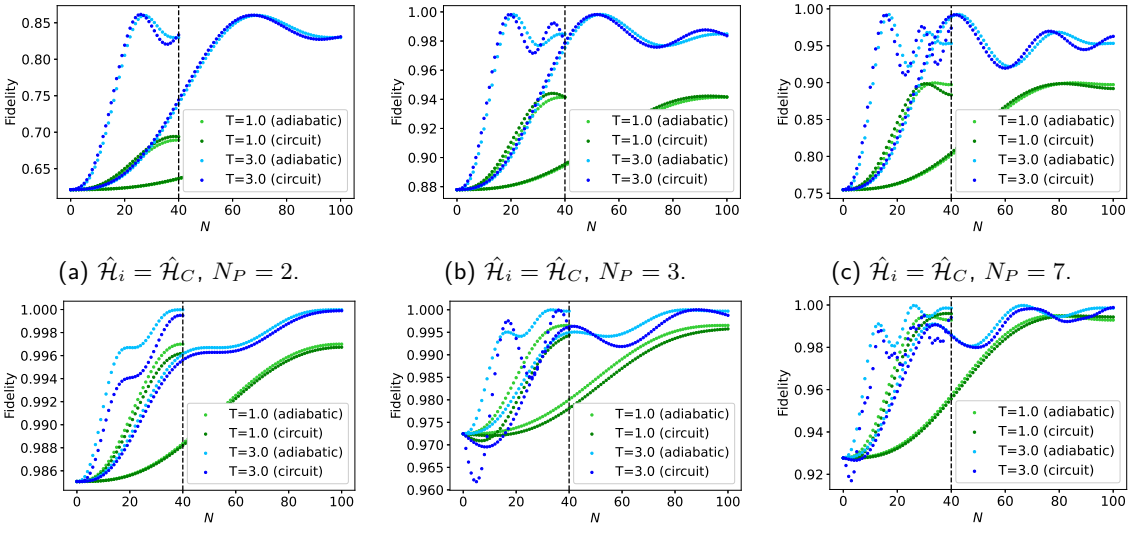

(a) $\hat{\mathcal{H}}_i = \hat{\mathcal{H}}_C$, $N_P = 2$. (b) $\hat{\mathcal{H}}_i = \hat{\mathcal{H}}_C$, $N_P = 3$. (c) $\hat{\mathcal{H}}_i = \hat{\mathcal{H}}_C$, $N_P = 7$.

(d) $\hat{\mathcal{H}}_i = \hat{\mathcal{H}}_K$, $N_P = 2$. (e) $\hat{\mathcal{H}}_i = \hat{\mathcal{H}}_K$, $N_P = 3$. (f) $\hat{\mathcal{H}}_i = \hat{\mathcal{H}}_K$, $N_P = 7$.

Figure 8: Comparison between adiabatic evolutions and trotter evolutions for different $\hat{\mathcal{H}}_i$ and N_P detailed in each subcaption. For each example, comparison for two different periods T and number of steps N are displayed.

It should be noted that for all cases a fidelity greater than 95% is achieved at least with an evolution period of $T = 3$, except for the first one, see Fig.8a. This case corresponds to an evolution starting from $\hat{\mathcal{H}}_C$ with an even number of particles. As mentioned above, this is the most unfavorable case.

Fig.9 shows the fidelity achieved for different examples depending on T and δt. Fig.9a explores the T, δt space for the example $t = 0 \to 1$, $U = 1$ with $N_P = 2$. In this example a maximum of $\approx 85\%$ is achieved. This low fidelity is due to the fact that, as mentioned above, when $\hat{\mathcal{H}}_i = \hat{\mathcal{H}}_C$ and the number of particles is even, the starting state has an overlap

of $\approx 62\%$ with the target state. This is why a very high fidelity is not obtained with a reasonable number of steps. Fig.9b analyzes the case of $t = 0 \to 1$, $U = 1$ with $N_P = 3$. Since there is an odd number of particles, we do not have the problem of the previous case since the initial overlap is of $\approx 88\%$. For practically all pairs of T and δt values the fidelity achieved is high for $T > 2.0$. However, a fidelity of $\approx 100\%$ is not reached at any time for these values.

In Fig.9c and Fig.9d the calculation is performed for the problem $U = 0 \to 1$, $t = 1$ with $N_P = 2$ and $N_P = 3$, respectively. After a certain period $T = 1$, the fidelity reaches 100%, but oscillations occur, so that it does not remain at 100% for all values of T, but oscillates between $\approx 97\%$ and 100%. In addition, it can be seen that for smaller δt values fidelities are higher. This pattern of oscillations is presented in a similar way in both figures. However, Fig.9c shows higher overall fidelities than Fig.9d. This may be because the initial overlap is $\approx 99\%$ and $\approx 97\%$ respectively.

In order to improve the fidelity of Fig.9a so that it is comparable to the rest, larger periods and shorter time steps are required, and therefore also many more steps N. This obviously implies a considerable increase in the depth of the circuit. This is the main motivation for introducing shortcuts to adiabaticity. A comparison between using and not using STA is shown below.

Figs.10a and 10b show the fidelity achieved as a function of the number of trotter steps N for $\delta t = 0.01,\ 0.1,\ 0.5$. As N increases, the value of T increases. Fig.10a shows that the fidelity grows slowly with N and cannot reach $\approx 100\%$ fidelity with $N < 40$ and $\delta t < 0.5$. In Fig.10b higher fidelities are reached because of the odd number of particles. Even so, at least 20 Trotter steps would be needed for $\delta t = 0.5$ to reach $\approx 100\%$ fidelity.

Fig.10a also shows the fidelity achieved when using STA considering only the first-order term in Ec.(20). The result is a fidelity of $\approx 100\%$ for only 4 trotter steps. In Fig.10b it is considered up to second-order term in Ec.(20). For $l = 1$ the adiabatic potential is not accurate enough and reaches fidelities that are exceeded by the curve without STA with $\delta t = 0.5$. However, with $l = 2$ the results improve significantly.

Although the results shown are for 2 sites, the entire algorithm is generalized for any number of sites except for the initial state preparation. That is why it has also been tested to work for systems of more sites with several particles. Cirq allows to create a circuit that evolves an arbitrary state different from $|0 \cdots 0\rangle$. We use this function to test the adiabatic evolution and the measurement for an initial state calculated with exact diagonalization.

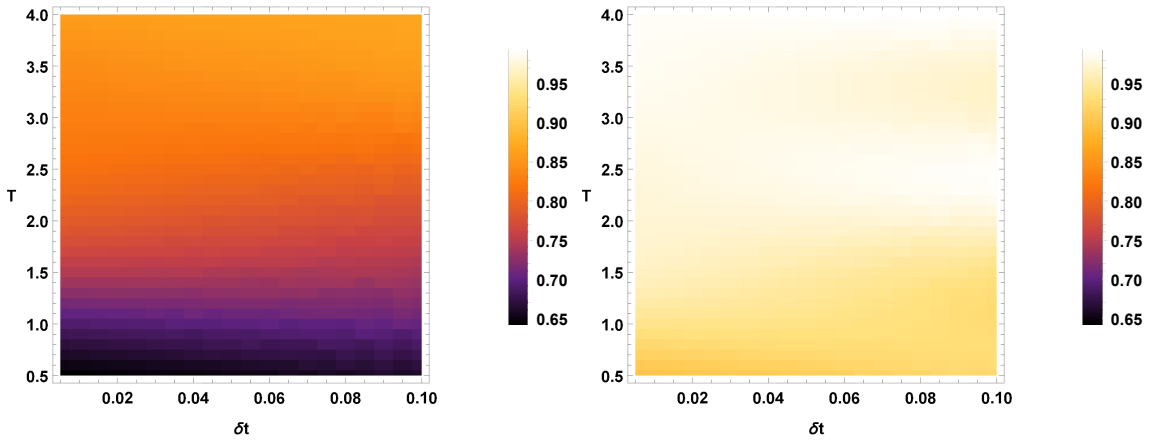

(a) $\hat{\mathcal{H}}_i = \hat{\mathcal{H}}_C$, $N_P = 2$, $\mathcal{F}_i \approx 62\%$

(b) $\hat{\mathcal{H}}_i = \hat{\mathcal{H}}_C$, $N_P = 3$, $\mathcal{F}_i \approx 88\%$

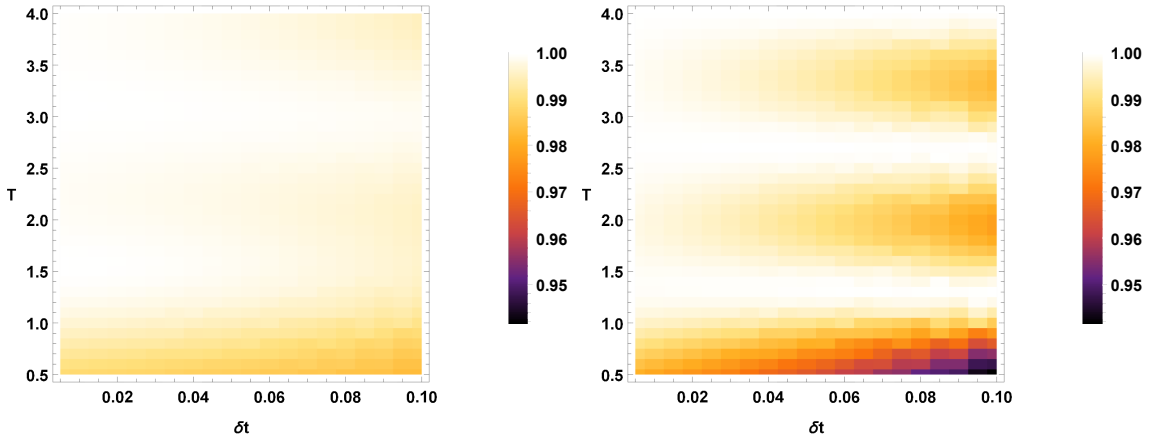

(c) $\hat{\mathcal{H}}_i = \hat{\mathcal{H}}_K$, $N_P = 2$, $\mathcal{F}_i \approx 99\%$

(d) $\hat{\mathcal{H}}_i = \hat{\mathcal{H}}_K$, $N_P = 3$, $\mathcal{F}_i \approx 97\%$

Figure 9: Fidelity achieved in the circuit evolution for problems with (a,b) $\hat{\mathcal{H}}_i = \hat{\mathcal{H}}_C$ and (c,d) $\hat{\mathcal{H}}_i = \hat{\mathcal{H}}_K$ considering systems of different sizes.

Despite the better results obtained using STA, the price to pay by introducing the counterdiabatic term is reflected in an increase in the circuit depth of a trotter step. For example, in the case of $N_P = 2$ the number of extra Pauli strings to consider in the Hamiltonian is 16. That means an added depth to a trotter step of 128. With what we have already commented we have a total depth in the evolution to reach $\approx 100\%$ of 6240 without using STA and 1136 using STA. In the case of $N_P = 5$ without using STA we have a depth of 29000. While if we use STA we have 8964 (for $l = 1$), 12128 (for $l = 2$). In view of this results, it is more advantageous (for these cases) then to use STA, both in terms of fidelity and in terms of circuit depth.

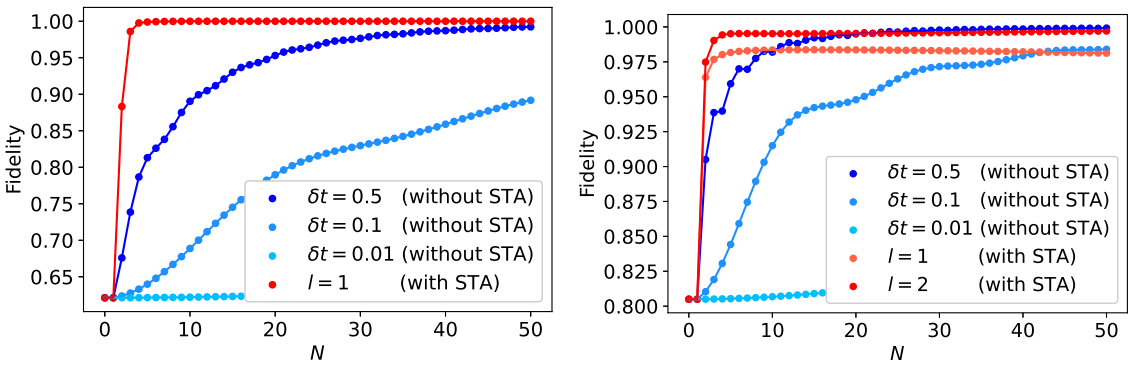

(a) $N_P = 2$ (b) $N_P = 5$

Figure 10: Fidelity achieved as a function of the number of trotter steps N for a fixed δt without using STA. Note that as N increases, T is increasing. The fidelity when using STA is also plotted. For $N_P = 2$ we have taken $l = 1$ and for $N_P = 5$ we have taken $l = 1, 2$. All points corresponding to STA have been calculated with $\delta t = 0.01$.

5 Conclusions

In this work, an adiabatic quantum algorithm has been constructed to obtain the ground state of the one-dimensional Bose-Hubbard Hamiltonian. The code used to describe all the circuits is the Gray code. First, a circuit has been constructed to prepare the ground state of both the Coulomb term $\hat{\mathcal{H}}_C$ and the kinetic term $\hat{\mathcal{H}}_K$, seeing a great advantage for the case of the former in terms of depth. Then the evolution operator has been Trotterized and a concatenation of circuits has been implemented, one for each exponential Pauli string. For each Trotter step we have analyzed the scaling as a function of the number of particles. Since the farther the initial state is from the target state the more trotter steps will be needed to reach a given fidelity, we have concluded that the best case is to start from the $\hat{\mathcal{H}}_K$ ground state, which is closer to the target one. In the measurement part we have proposed a strategy to simultaneously measure commuting terms by implementing circuits with a constant depth with the number of particles.

An STA method has been implemented to improve the adiabatic evolution of the system when $\hat{\mathcal{H}}_i = \mathcal{H}_K$. For this purpose the approximate CD driving has been calculated using the nested commutator method. With this, an improvement in both the evolution time and the required circuit depth has been seen for some examples, thus demonstrating the advantages of using this method. In addition, it has been shown that as the number of qubits increases, the fidelity can be further improved with higher-order terms at the cost of depth. These examples highlight the significant improvement that occurs when STA is introduced, decreasing quantum resources and execution time (more in line with device coherence time) [HPD+21].

One pending point is to study the scaling of a Trotter step when the counterdiabatic term is added, in order to make a comparison of the advantages and disadvantages of introducing STA in the algorithm for any number of sites and particles.

All results presented in this manuscript correspond to systems of N_P particles at two sites. For this particular case we have found that all steps involved in the simulation (i.e. the preparation of the initial state, evolution and measurement) can be performed with polynomial complexity: the depth in each part of the circuit scales polynomially with the system size. However, both adiabatic evolution and measurement are implemented for any number of sites. What is not easily generalizable for N_S is the preparation of the initial

state, but we can say that the depth of the circuit will be increased by having to prepare more complicated states. Future work remains to implement these circuits and to analyze the scaling of the complete algorithm as a function of N_P and N_S.

As explained in the main text, the motivation for using the Gray code is that it is suitable for representing the kinetic term. However, according to [SMK+20], in the BH model, the number operator $\hat{n}$ is usually more efficient in SB, while the hopping term, $\hat{a}_i^\dagger \hat{a}_{i+1} + \hat{a}_{i+1}^\dagger \hat{a}_i$ is usually more efficient in the Gray coding. As a future work, it could be studied if changing the encoding in each Trotter step implies more or less depth in the circuit than using always the same encoding.

Bibliography

[BCLK+21] Kishor Bharti, Alba Cervera-Lierta, Thi Ha Kyaw, Tobias Haug, Sumner Alperin-Lea, Abhinav Anand, Matthias Degroote, Hermanni Heimonen, Jakob S Kottmann, Tim Menke, et al. Noisy intermediate-scale quantum (nisq) algorithms. *arXiv preprint arXiv:2101.08448*, 2021.

[CPSP19] Pieter W Claeys, Mohit Pandey, Dries Sels, and Anatoli Polkovnikov. Floquet-engineering counterdiabatic protocols in quantum many-body systems. *Physical Review Letters*, 123(9):090602, 2019.

[HPD+21] Narendra N Hegade, Koushik Paul, Yongcheng Ding, Mikel Sanz, Francisco Albarrán-Arriagada, Enrique Solano, and Xi Chen. Shortcuts to adiabaticity in digitized adiabatic quantum computing. *Physical Review Applied*, 15(2):024038, 2021.

[KSMP17] Michael Kolodrubetz, Dries Sels, Pankaj Mehta, and Anatoli Polkovnikov. Geometry and non-adiabatic response in quantum and classical systems. *Physics Reports*, 697:1–87, 2017.

[PLOPO21] Oscar Perdomo, Vicente Leyton-Ortega, and Alejandro Perdomo-Ortiz. Entanglement types for two-qubit states with real amplitudes. *Quantum Information Processing*, 20(3):1–12, 2021.

[POPSSR+22] Axel Pérez-Obiol, Adrián Pérez-Salinas, Sergio Sánchez-Ramírez, Bruna GM Araújo, and Artur Garcia-Saez. Adiabatic quantum algorithm for artificial graphene. *arXiv preprint arXiv:2204.03013*, 2022.

[RGLJD17] David Raventós, Tobias Graß, Maciej Lewenstein, and Bruno Juliá-Díaz. Cold bosons in optical lattices: a tutorial for exact diagonalization. *Journal of Physics B: Atomic, Molecular and Optical Physics*, 50(11):113001, 2017.

[SMK+20] Nicolas PD Sawaya, Tim Menke, Thi Ha Kyaw, Sonika Johri, Alán Aspuru-Guzik, and Gian Giacomo Guerreschi. Resource-efficient digital quantum simulation of d-level systems for photonic, vibrational, and spin-s hamiltonians. *npj Quantum Information*, 6(1):1–13, 2020.

[SOKG03] Rolando Somma, Gerardo Ortiz, Emanuel Knill, and James Gubernatis. Quantum simulations of physics problems. *International Journal of Quantum Information*, 1(02):189–206, 2003.

[SP13] Mehdi Saeedi and Massoud Pedram. Linear-depth quantum circuits for n-qubit toffoli gates with no ancilla. *Physical Review A*, 87(6):062318, 2013.

[STC22] Benjamin F Schiffer, Jordi Tura, and J Ignacio Cirac. Adiabatic spectroscopy and a variational quantum adiabatic algorithm. *PRX Quantum*, 3(2):020347, 2022.

[TIMG+13] Erik Torrontegui, Sara Ibáñez, Sofia Martínez-Garaot, Michele Modugno, Adolfo del Campo, David Guéry-Odelin, Andreas Ruschhaupt, Xi Chen, and Juan Gonzalo Muga. Shortcuts to adiabaticity. In *Advances in atomic, molecular, and optical physics*, volume 62, pages 117–169. Elsevier, 2013.

A Bose-Hubbard derivations

In this Appendix the ground state of each term of the Hamiltonian of the one-dimensional Bose-Hubbard model will be derived in detail for a general case of N_S sites and N_P particles. The expressions obtained will be referenced by the main text.

A.1 Ground state of $\hat{\mathcal{H}}_C$

When $t = 0$, the surviving term in Ec.(1) is,

$$\hat{\mathcal{H}}_C = \frac{U}{2}\sum_{i=1}^{N_S}\hat{n}_i(\hat{n}_i - 1). \tag{A.1}$$

The eigenstates of this Hamiltonian are the Fock basis states as it is diagonal in that basis. When $U \geq 0$, the interaction between particles is repulsive and it follows that they are arranged in the most dispersed way possible, i.e, when the number of particles is divisible by the number of sites, each site contains N_P/N_S particles and the eigenvalues are non-degenerate. When this is not the case, there is degeneracy. In the specific case of two sites, we have

$$|\Psi_C(N_P)\rangle = \left|\frac{N_P}{2}\,\frac{N_P}{2}\right\rangle, \tag{A.2}$$

for an even number of particles, and

$$|\Psi_C(N_P)\rangle = \alpha\left|\frac{N_P}{2} - \frac{1}{2}\,\frac{N_P}{2} + \frac{1}{2}\right\rangle + \beta\left|\frac{N_P}{2} + \frac{1}{2}\,\frac{N_P}{2} - \frac{1}{2}\right\rangle, \tag{A.3}$$

for an odd number of particles. $\alpha^2 + \beta^2 = 1$ is verified. Starting from this state, in the adiabatic evolution the kinetic term will slowly turn on. Specifically, in the first Trotter step the Hamiltonian is given by

$$\hat{\mathcal{H}} = \hat{\mathcal{H}}_C + \epsilon\hat{\mathcal{H}}_K, \tag{A.4}$$

where $\epsilon = \delta t/N = 1/T$. The matrix to be diagonalized is as follows

$$\begin{pmatrix} \left\langle \frac{N_P-1}{2}\,\frac{N_P+1}{2}\right|\hat{\mathcal{H}}_K\left|\frac{N_P-1}{2}\,\frac{N_P+1}{2}\right\rangle & \left\langle \frac{N_P-1}{2}\,\frac{N_P+1}{2}\right|\hat{\mathcal{H}}_K\left|\frac{N_P+1}{2}\,\frac{N_P-1}{2}\right\rangle \\ \left\langle \frac{N_P+1}{2}\,\frac{N_P-1}{2}\right|\hat{\mathcal{H}}_K\left|\frac{N_P-1}{2}\,\frac{N_P+1}{2}\right\rangle & \left\langle \frac{N_P+1}{2}\,\frac{N_P-1}{2}\right|\hat{\mathcal{H}}_K\left|\frac{N_P+1}{2}\,\frac{N_P-1}{2}\right\rangle \end{pmatrix}. \tag{A.5}$$

By calculating these elements we have

$$\begin{pmatrix} 0 & -t\frac{N_P+1}{2} \\ -t\frac{N_P+1}{2} & 0 \end{pmatrix}, \tag{A.6}$$

whose eigenvalues are $\mp t(N_P+1)/2$. Its eigenvectors are

$$|\pm\rangle = \frac{1}{\sqrt{2}}\left(\left|\frac{N_P-1}{2}\,\frac{N_P+1}{2}\right\rangle \pm \left|\frac{N_P-1}{2}\,\frac{N_P+1}{2}\right\rangle\right), \tag{A.7}$$

respectively.

Considering $|+\rangle$ as the initial state, when the first Trotter step is applied, we have

$$e^{-i\hat{\mathcal{H}}_C\delta t - i\hat{\mathcal{H}}_K\delta t/N}\,|+\rangle\,. \tag{A.8}$$

If $\delta t/N$ is small, according to first-order perturbation theory, $|+\rangle$ is an eigenstate of $e^{-i\hat{\mathcal{H}}_C\delta t - i\hat{\mathcal{H}}_K\delta t/N}$ and that is why we can consider it as our initial state.

A.2 Ground state of $\hat{\mathcal{H}}_\mathbf{K}$

When $U = 0$, the surviving term in Ec.(1) is,

$$\hat{\mathcal{H}}_K = -t\sum_{\langle ij\rangle}\left(\hat{a}_i^\dagger\hat{a}_j + \hat{a}_j^\dagger\hat{a}_i\right). \tag{A.9}$$

In the first neighbors approach we have

$$\hat{\mathcal{H}}_K = -t\sum_{i=0}^{N_S-1}\left(\hat{a}_i^\dagger\hat{a}_{i+1} + \hat{a}_{i+1}^\dagger\hat{a}_i\right), \tag{A.10}$$

and periodic boundary conditions are imposed such that $\hat{a}_{N_S} \equiv \hat{a}_0$.

The Fourier transform can be performed on the operators $\hat{a}_j^\dagger$ and $\hat{a}_k$, so that

$$\hat{a}_j^\dagger = \frac{1}{\sqrt{N_S}}\sum_{j'=0}^{N_S-1} e^{-ijj'\frac{2\pi}{N_S}}\hat{b}_j^\dagger, \qquad \hat{a}_k = \frac{1}{\sqrt{N_S}}\sum_{k'=0}^{N_S-1} e^{ikk'\frac{2\pi}{N_S}}\hat{b}_j, \tag{A.11}$$

where $\hat{b}_j^\dagger$, $\hat{b}_j$ are momentum operators: they create/annihilate a particle with momentum j.

Substituting both expressions in Ec.(A.10)

$$\begin{aligned}
\hat{\mathcal{H}}_K &= -t\sum_{j=0}^{N_S-1}\frac{1}{N_S}\sum_{j',k'=0}^{N_S-1} e^{i[(j+1)k'-jj']\frac{2\pi}{N_S}}\hat{b}_{j'}^\dagger\hat{b}_{k'} + h.c. \\
&= -\frac{t}{N_S}\sum_{j',k'=0}^{N_S-1}\underbrace{\sum_{j=0}^{N_S-1} e^{i\frac{2\pi}{N_S}j(k'-j')}}_{N_S\cdot\delta_{k'j'}} e^{i\frac{2\pi}{N_S}k'}\hat{b}_{j'}^\dagger\hat{b}_{k'} + h.c. \\
&= -t\sum_{j'=0}^{N_S-1} e^{i\frac{2\pi}{N_S}j'}\hat{b}_{j'}^\dagger\hat{b}_{k'} + h.c. \\
&= -t\sum_{j=0}^{N_S-1} 2\cos\left(\frac{2\pi}{N_S}j\right)\hat{b}_j^\dagger\hat{b}_j,
\end{aligned} \tag{A.12}$$

where

$$\hat{b}_j^\dagger = \frac{1}{\sqrt{N_S}}\sum_{j'=0}^{N_S-1} e^{ijj'\frac{2\pi}{N_S}}\hat{a}_j^\dagger, \qquad \hat{b}_k = \frac{1}{\sqrt{N_S}}\sum_{k'=0}^{N_S-1} e^{-ikk'\frac{2\pi}{N_S}}\hat{a}_j. \tag{A.13}$$

In view of Ec.(A.13) we have that the eigenstates are of the form $\left(\hat{b}_j^\dagger\right)^{N_P}|\underbrace{00\cdots0}_{N_S}\rangle$, with eigenvalues $-2t\cos(2\pi j/N_S)$. The ground state corresponds to $j = 0$. Therefore, for any number of sites and particles the ground state is non-degenerate. Its energy is $-2t$ and its (unnomalized) eigenvector is given by

$$\left(\hat{b}_0^\dagger\right)^{N_P} |\underbrace{00\cdots0}_{N_S}\rangle = \sum_{k_1,k_2\cdots k_{N_S}}^{N_P} \binom{N_P}{k_1 k_2 \cdots k_{N_S}} \sqrt{k_1!}\sqrt{k_s!}\cdots\sqrt{k_{N_S}!}\,|k_1 k_2 \cdots k_{N_S}\rangle\,, \quad \text{(A.14)}$$

where $k_1 + k_2 + \cdots + k_{N_S} = N_P$, and $\hat{b}_0^\dagger$ is given by

$$\hat{b}_0^\dagger = \frac{1}{\sqrt{N_S}} \sum_{j'=0}^{N_S-1} \hat{a}_{j'}^\dagger. \quad \text{(A.15)}$$

In the specific case of two sites, we have the (unnormalized) state

$$|\Psi_K\rangle = \sum_{i=0}^{N_P} \binom{N_P}{i} \sqrt{i!}\sqrt{(N_P-i)!}\,|i\ N_P - i\rangle\,. \quad \text{(A.16)}$$

For instance,

$$|\Psi_K(N_P=4)\rangle = \frac{1}{4}|0\,4\rangle + \frac{1}{2}|1\,3\rangle + \frac{\sqrt{6}}{4}|2\,2\rangle + \frac{1}{2}|3\,1\rangle + \frac{1}{4}|4\,0\rangle\,. \quad \text{(A.17)}$$

B Number of measurements

In this Appendix we estimate an upper bound for the number of measurements needed to obtain one value of the final state energy, i.e., the number of groups of Hamiltonian terms that can be simultaneously measured.

As mentioned in Section 3.4, only one measurement is needed to compute one single value of the energy due to the Coulomb term, $\langle\hat{\mathcal{H}}_C\rangle$. However, for the kinetic term we can only simultaneously measure $\{\langle\cdots X_i\cdots X_j\cdots\rangle,\ \langle\cdots Y_i\cdots Y_j\cdots\rangle\}$ and $\{\langle\cdots X_i\cdots Y_j\cdots\rangle,\ \langle\cdots Y_i\cdots X_j\cdots\rangle\}$. Note that in the case of $N_S = 2$, Kronecker products $\underbrace{\hat{\sigma}^{(k)}\otimes\cdots\otimes\hat{\sigma}^{(k')}}_{n_q}\underbrace{\hat{\sigma}^{(l)}\otimes\cdots\otimes\hat{\sigma}^{(l')}}_{n_q}$ have only one sigma matrix $\hat{\sigma}^{(+)}$ or $\hat{\sigma}^{(-)}$ at the position of one of the first site qubits and another at the same position of one of the second site qubits. This is because in Gray only one digit changes between consecutive states (those appearing in $\hat{\mathcal{H}}_K$). Therefore, there will be at most $4n_q$ terms to measure (the 4 comes from the possible combinations XX, XY, YX, YY). But since we have two groups that can be measured simultaneously, we are left with $N_q = n_q/2$ measurements. In total, then, a maximum of $1 + N_q$ measurements will be required.

C $\hat{\mathcal{H}}_K$ ground state preparation

In this Appendix we present a possible algorithm to prepare the ground state of the kinetic term of the Bose-Hubbard Hamiltonian with a quantum circuit. The coding used to prepare the state is the Gray code. First, a way to prepare any two-qubit state will be presented [PLOPO21] and then it will be explained how to use it to prepare the ground state of the kinetic term with any value of N_P and $N_S = 2$. Finally, we will study how the depth of this circuit scales as a function of the number of particles.

C.1 Preparing any two-qubit state

If we want to obtain $|00\rangle$ from any two-qubit state, the quantum circuit is given by the following scheme:

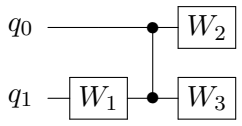

Figure 11: Circuit that transforms any two-qubit state $|\Psi_0\rangle$ into $|00\rangle$. Only three one-qubit gates and one controlled-Z are required.

With this circuit the state $|00\rangle$ is obtained from any state

$$|\Psi_0\rangle = \xi_0 |00\rangle + \xi_1 |01\rangle + \xi_2 |10\rangle + \xi_3 |11\rangle .$$

W_1, W_2 and W_3 are one-qubit gates defined from three unitary matrices of the form:

$$W(x,y) = \frac{1}{\sqrt{x^2+y^2}} \begin{pmatrix} x & y \\ -y^* & x^* \end{pmatrix}.$$

First, let's define two vectors A_1 and A_2 which are given by

$$A_1 = (\xi_0, \xi_1), \qquad\qquad A_2 = (\xi_2, \xi_3),$$

and parameter k:

$$k = \begin{cases} \frac{A_2}{A_1} & if \quad \langle A_1|A_2\rangle = 0, \\ -\frac{A_2}{A_1}\frac{\langle A_1|A_2\rangle}{\langle A_1|A_2\rangle} & if \quad \langle A_1|A_2\rangle \neq 0. \end{cases}$$

Unitary matrix W_1 is defined as

$$W_1 = W(\xi_3 - k\xi_1, \xi_2^* - k^*\xi^*)^T,$$

so that after the application of W_1 and controlled-Z in $|\Psi_0\rangle$, we have

$$|\Psi_1\rangle = CZ \cdot (\mathbb{I} \otimes W_1) |\Psi_0\rangle = \eta_0 |00\rangle + \eta_1 |01\rangle + \eta_2 |10\rangle + \eta_3 |11\rangle .$$

Unitary matrix W_2 is defined as

$$W_2 = W(\eta_1^*, \eta_3^*),$$

and after its application to $|\Psi_1\rangle$, we have

$$|\Psi_2\rangle = (W_2 \otimes \mathbb{I}) |\Psi_1\rangle = \gamma_0 |00\rangle + \gamma_1 |01\rangle + \gamma_2 |10\rangle + \gamma_3 |11\rangle .$$

W_3 is defined as

$$W_3 = W(\gamma_0^*, -\gamma_1^*)^T,$$

finally obtaining after its application the state $|\Psi_3\rangle = |00\rangle$.

If we implement this circuit in reverse, with the unitary matrices defining the gates now being their corresponding inverses (we use the notation $W^{-1} \equiv U$), we can prepare any two-qubit state.

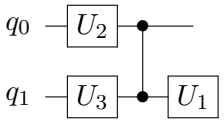

Figure 12: Circuit that prepares any two-qubit state. Only 3 gates of one qubit and one controlled-Z are required.

Let us now see how to prepare any two-qubit state if we have $m-2$ control qubits. The idea is that now all gates shown in Fig.12 are controlled by these qubits.

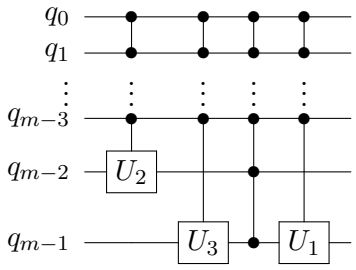

Figure 13: Circuit to prepare any two-qubit state with qubits q_{m-2} and q_{m-1} controlled by $m-2$ qubits. The state obtained is $|q_0\, q_1 \cdots q_{m-2}\rangle\, (\xi_0 |00\rangle + \xi_1 |01\rangle + \xi_2 |10\rangle + \xi_3 |11\rangle)$. If we want one of the control qubits to be in $|0\rangle$ just add an X gate at the beginning and end of the circuit in that qubit.

In general any gate controlled by $m-1$ qubits (m-controlled gate) can be decomposed into two one-qubit gates and two m-qubit Toffoli gates. An m-qubit Toffoli gate can be decomposed into two-qubit controlled-rotation gates in such a way that its circuit depth is $8m-20$ [SP13]. Circuit in Fig.14b then has a depth of $2+2(8m-20) = 16m-38$.

Figure 14: (a) An m-controlled U gate can be decomposed into (b) two m-qubit Toffoli gates and two one-qubit gates V and $V^\dagger$, where V is the square root of U.

Let us then calculate the depth of the circuit in Fig.13. There are three $(m-1)$-controlled U gates and one m-controlled Z gate. Therefore, we have $3\,[16\,(m-1)-38] + 16m - 38 = 64m - 200$.

C.2 Algorithm

The (unnormalized) ground state of $\hat{\mathcal{H}}_K$ is given

$$|\Psi_K(N_P)\rangle = \sum_{i=0}^{N_P} \binom{N_P}{i} \sqrt{i!}\sqrt{(N_P-i)!}\,|i, N_P-i\rangle\,, \tag{C.1}$$

where $|i, N_P - i\rangle$ belongs to the Fock basis $\{|n_1, n_2\rangle\}$.

Ultimately, we have to prepare a state of the form

$$|\Psi_K(N_P)\rangle = \sum_{i=0}^{N_P} c_i\,|i, N_P-i\rangle\,. \tag{C.2}$$

The idea is to prepare the first part of the state (to prepare the state by ignoring the qubits corresponding to the second site), i.e

$$|\Phi\rangle = \left(\sum_{i=0}^{N_P} c_i\,|i^{(G)}\rangle\right) \underbrace{|00\cdots0\rangle}_{n_q}, \tag{C.3}$$

working with n_q qubits and to have n_q additional qubits to complete the second part. For this task, we add several n-qubit Toffoli gates. Control qubits are those describing the state of the first site and target qubits those corresponding to the second site. It is then a task of adding as many n-qubit Toffoli gates as necessary to obtain the desired superposition state.

To help the reader, we explain in detail below how the algorithm works for the case of $N_P = 6$.

The initial state we have to prepare is

$$\begin{aligned} |\Psi_K^{(G)}(N_P=6)\rangle &= \frac{1}{8}|000\rangle|101\rangle + \frac{1}{4}\sqrt{\frac{3}{2}}|001\rangle|111\rangle + \frac{\sqrt{15}}{8}|011\rangle|110\rangle \\ &+ \frac{\sqrt{5}}{4}|010\rangle|010\rangle + \frac{\sqrt{15}}{8}|110\rangle|011\rangle + \frac{1}{4}\sqrt{\frac{3}{2}}|111\rangle|001\rangle \\ &+ \frac{1}{8}|101\rangle|000\rangle \end{aligned} \tag{C.4}$$

To prepare the first part of the state

$$\begin{aligned} |\phi_0\rangle &= \left(\frac{1}{8}|000\rangle + \frac{1}{4}\sqrt{\frac{3}{2}}|001\rangle + \frac{\sqrt{15}}{8}|011\rangle + \frac{\sqrt{5}}{4}|010\rangle \right. \\ &+ \left. \frac{\sqrt{15}}{8}|110\rangle + \frac{1}{4}\sqrt{\frac{3}{2}}|111\rangle + \frac{1}{8}|101\rangle\right)|000\rangle \end{aligned} \tag{C.5}$$

we proceed as follows[4]:

- (Step 1) An R_y gate is applied in qubit q_0,

$$|000\rangle \to \alpha\,|000\rangle + \beta\,|100\rangle\,.$$

[4]Qubits to be worked with in each step are shown in blue.

- (Step 2) With the last two qubits, we move to a new state emerging from $|000\rangle$ (q_0 as a control qubit, in red), for which the gates U_1, U_2 and U_3 are defined in such a way that,

$$\alpha\,|000\rangle \to \frac{1}{8}\,|000\rangle + \frac{1}{4}\sqrt{\frac{3}{2}}\,|001\rangle + \frac{\sqrt{5}}{4}\,|010\rangle + \frac{\sqrt{15}}{8}\,|011\rangle\,.$$

- (Step 3) With the last two qubits, we move to another new state emerging from $|100\rangle$ (q_0 as a control qubit, in red), for which the gates U_1, U_2 and U_3 are defined in such a way that,

$$\beta\,|100\rangle \to \frac{1}{8}\,|101\rangle + \frac{\sqrt{15}}{8}\,|110\rangle + \frac{1}{4}\sqrt{\frac{3}{2}}\,|111\rangle\,.$$

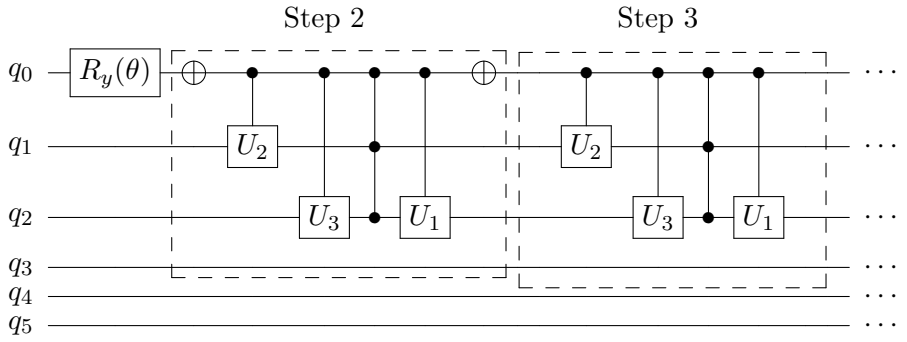

Figure 15: Circuit that prepares $|\phi_0\rangle$. Note that in step 2 a gate X is added at the beginning and end of the circuit since the control qubit q_0 is in $|0\rangle$.

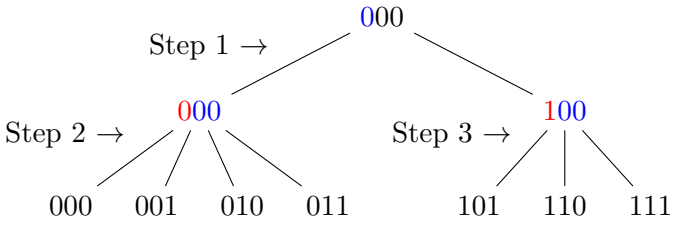

Figure 16: Diagram that helps to visualize the designed algorithm. Qubits worked in each step are shown in blue and control qubits in red. Applying the R_y gate to q_0 in the first step generates a superposition of two states, $|000\rangle$ and $|100\rangle$. In the second step one of them, $|000\rangle$, becomes a 4-state superposition. In the third step $|100\rangle$ becomes a 3-state superposition. Finally we have the desired 7-state superposition, Ec.(C.4).

Then, in order to modify the qubits of the second site, we have to do the following mapping:

$$
\begin{aligned}
|000\rangle\,|000\rangle &\rightarrow |000\rangle\,|101\rangle \;\; (a)\\
|001\rangle\,|000\rangle &\rightarrow |001\rangle\,|111\rangle \;\; (b)\\
|011\rangle\,|000\rangle &\rightarrow |011\rangle\,|110\rangle \;\; (c)\\
|010\rangle\,|000\rangle &\rightarrow |010\rangle\,|010\rangle \;\; (d)\\
|110\rangle\,|000\rangle &\rightarrow |110\rangle\,|011\rangle \;\; (e)\\
|111\rangle\,|000\rangle &\rightarrow |111\rangle\,|001\rangle \;\; (f)\\
|101\rangle\,|000\rangle &\rightarrow |101\rangle\,|000\rangle \;\; (g)
\end{aligned}
$$

There seems to be no simple way to build a generalizable circuit for N_P particles that does this type of mapping. That is why we use n-qubit Toffoli gates. In red are the control qubits, which correspond to those at the first site. In green appear the qubits of the second site on which the gates are applied, i.e, those that have to change their state from $|0\rangle$ to $|1\rangle$. As many gates of this type are applied as qubits that have to change state. X gates are also added in the qubits of the first site with state $|0\rangle$. In this case 11 4-qubit Toffoli gates are needed.

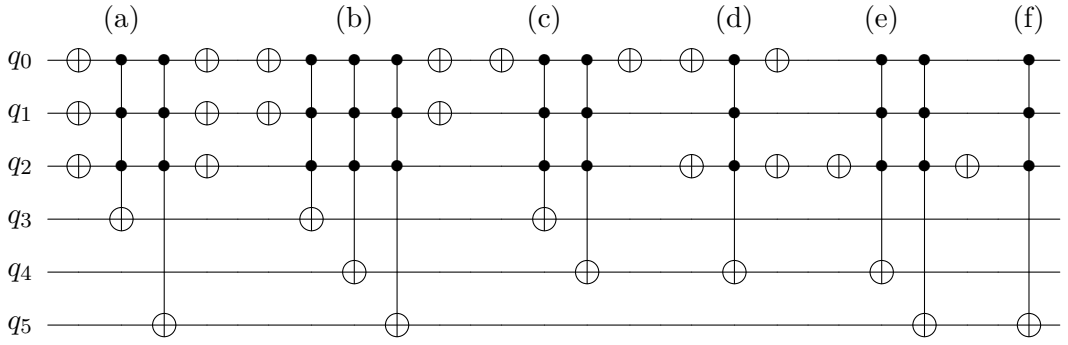

Figure 17: Circuit that completes the second part by adding 11 4-qubit Toffoli gates. Two X gates acting in succession on the same qubit are cancelled. However, they have been put in the figure for illustrative purposes and to facilitate understanding.

The general scheme of the algorithm for any number of particles can be inferred from this example. Let $N_q = N_S \cdot n_q$ be the total number of qubits, where n_q is the number of qubits needed to represent one site. First $n_q - 2$ controlled-R_y gates are applied on the first $n_q - 2$ qubits: one rotation in q_0, two rotations on q_1 controlled by q_0, four rotations on q_2 controlled by q_0 and q_1 and so on. Then 2^{n_q-2} circuits like the one in Fig.13 controlled by the $n_q - 2$ qubits are concatenated. Finally, as many $(n_q + 1)$-qubit Toffoli gates are added as many qubits of the second site have to modify their state from $|0\rangle$ to $|1\rangle$ (for all the states that make up the initial state).

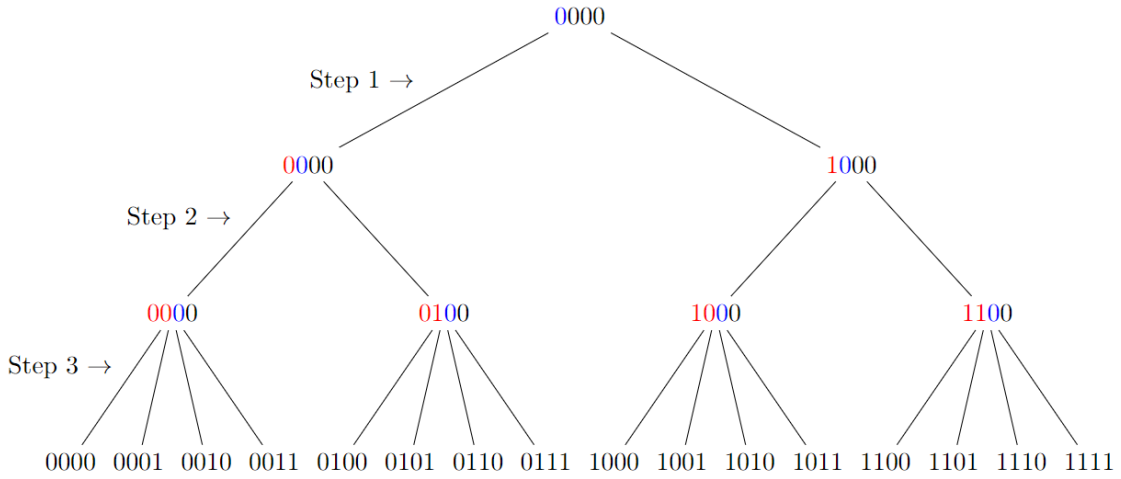

Figure 18: Diagram that helps to visualize the designed algorithm. Qubits worked in each step are shown in blue and control qubits in red. Applying the R_y gate to q_0 in the first step generates a superposition of two states, $|000\rangle$ and $|100\rangle$. In the second step, a rotation gate in q_1 controlled by q_0 in state $|0\rangle$ and another rotation gate in q_1 controlled by q_0 in state $|1\rangle$ are applied. In the third step, 2^{n_q-2} circuits as shown in Fig.13 are applied to obtain the desired superposition state.

Let us estimate how the depth of the circuit scales as a function of the number of particles. Applying the controlled rotations we have $1+4+\sum_{n=3}^{n_q-2} 2^{n-1}(16n-38)$. With the application of the 2^{n_q-2} circuits as shown in Fig.13 we have $(2^{n_q-2}-1)\cdot[2+64n_q-200]+2^{n_q-2}\cdot(64n_q-200)$. This calculation is an upper bound for the depth of this part since for a fixed number of qubits, depending on the number of particles, sometimes fewer such circuits are needed to build the state. To simplify the calculation when adding the (n_q+1)-qubit Toffoli gates let us assume that all qubits in the second site have to change their state from $|0\rangle$ to $|1\rangle$, i.e., as if the mapping example were like this

$$
\begin{aligned}
|000\rangle\,|000\rangle &\rightarrow |000\rangle\,|111\rangle \;\; (a)\\
|001\rangle\,|000\rangle &\rightarrow |001\rangle\,|111\rangle \;\; (b)\\
|011\rangle\,|000\rangle &\rightarrow |011\rangle\,|111\rangle \;\; (c)\\
|010\rangle\,|000\rangle &\rightarrow |010\rangle\,|011\rangle \;\; (d)\\
|110\rangle\,|000\rangle &\rightarrow |110\rangle\,|011\rangle \;\; (e)\\
|111\rangle\,|000\rangle &\rightarrow |111\rangle\,|001\rangle \;\; (f)\\
|101\rangle\,|000\rangle &\rightarrow |101\rangle\,|001\rangle \;\; (g)
\end{aligned}
$$

It would then be necessary to apply $\sum_{n=1}^{N_P} n_q(n)$ (n_q+1)-qubit Toffoli gates at the most. At most $2N_P$ layers of X gates are also added. The depth of this part is then calculated as $2N_P+[8(n_q+1)-20]\sum_{n=1}^{N_P} n_q(n)$.

If we add it all up, and write it as a function of the number of particles we get

$$
\mathcal{D}_K^{(\mathrm{IGS})} \leq 227 - 239N_P + 4\log_2 N_P\left[(-16+27N_P)+2N_P\log_2 N_P\right], \tag{C.6}
$$

that is, it scales polynomially with the number of particles.